The Astrophysical Journal Letters, 805:L12 (5pp), 2015 June 1 doi:10.1088/2041-8205/805/2/L12

DETECTION OF OH^+ IN TRANSLUCENT INTERSTELLAR CLOUDS: NEW ELECTRONIC TRANSITIONS AND PROBING THE PRIMARY COSMIC RAY IONIZATION RATE*

D. Zhao[1], G. A. Galazutdinov[2,3], H. Linnartz[1], and J. Krełowski[4]
[1] Sackler Laboratory for Astrophysics, Leiden Observatory, University of Leiden, PO Box 9513, 2300 RA Leiden, The Netherlands; zhao@strw.leidenuniv.nl
[2] Instituto de Astronomia, Universidad Catolica del Norte, Av. Angamos 0610, Antofagasta, Chile
[3] Pulkovo Observatory, Pulkovskoe Shosse 65, Saint-Petersburg 196140, Russia
[4] Center for Astronomy, Nicholas Copernicus University, Gagarina 11, Pl-87-100 Toruń, Poland
Received 2015 February 9; accepted 2015 April 6; published 2015 May 27

ABSTRACT

We present the detection of rotationally resolved electronic transitions in the OH^+ $A^3\Pi$–$X^3\Sigma^-$ (0, 0) and (1, 0) bands toward CD-32 4348, HD 63804, HD 78344, and HD 80077. These four translucent clouds have been studied in a recent Very Large Telescope/Ultraviolet and Visual Echelle Spectrograph observational run. In total, seven absorption features of OH^+ are detected, and six of them are identified here for the first time, providing a precise tool to trace OH^+ in translucent interstellar clouds. An improved set of line positions and oscillator strengths is compiled to support our data interpretation. A dedicated analysis of the observed features in individual targets yields an accurate determination of OH^+ column densities. The results are applied to estimate the primary cosmic ray ionization rate in the investigated translucent clouds, which yields a typical value of $\sim 1.0 \times 10^{-16}$ s^{-1}. In addition, following this work, two of the new interstellar features recently reported by Bhatt & Cami, at ~3572.65 and 3346.96 Å, can be identified as OH^+ absorption lines now.

Key words: ISM: clouds – ISM: lines and bands – ISM: molecules – ultraviolet: ISM

1. INTRODUCTION

The hydroxyl cation OH^+ plays a central role in the gas phase oxygen chemistry of the interstellar medium (ISM), in particular, in the gas phase formation scheme of water. Astrochemical models (see the recent reviews by van Dishoeck et al. 2013 and Tielens 2013 and references therein) suggest that the gas phase formation of water in the diffuse ISM is driven by ion-neutral reactions, starting from the formation of OH^+. This ion has also been suggested as an important diagnostic probe for the cosmic ray ionization rate in diffuse/translucent clouds (Gerin et al. 2010; Neufeld et al. 2010; Hollenbach et al. 2012). The astronomical detection of this ion, however, was only realized after 2010, using the Atacama Pathfinder Experiment (Wyrowski et al. 2010), the HIFI instrument on board the *Herschel Space Observatory* (Gerin et al. 2010; Neufeld et al. 2010) in the submillimeter region, and the Ultraviolet and Visual Echelle Spectrograph (UVES) of the Very Large Telescope (VLT) in the near-ultraviolet (UV; Krełowski et al. 2010). OH^+ has also been detected in emission with HIFI/Herschel (see, e.g., Barlow et al. 2013; van der Tak et al. 2013). These observations were immediately used to infer the cosmic ray ionization rate and to constrain the oxygen chemistry in the ISM (Hollenbach et al. 2012; Indriolo et al. 2012, 2015; van der Tak et al. 2013; Porras et al. 2014).

Thus far, observational detections of OH^+ in the near-UV domain only rely on one weak absorption line at 3583.76 Å with a central absorption depth that is typically less than 0.02 (Krełowski et al. 2010; Gredel et al. 2011; Porras et al. 2014). In this Letter, we present the detection of seven absorption lines of OH^+ $A^3\Pi$–$X^3\Sigma^-$ (0, 0) and (1, 0) bands in the spectra of four translucent interstellar clouds. A set of molecular parameters, including the newly calculated line oscillator strengths, is compiled to support our data analysis. A combined analysis of the known 3583.76 Å line and the newly identified features allows us to accurately determine OH^+ column densities, as well as to infer the primary cosmic ray ionization rate in translucent clouds.

2. OBSERVATIONS

Observations were made using UVES at the 8 m UT2 telescope (Paranal Observatory, ESO, Chile) from our observational run in 2014 March (program 092.C-0019(A)). Two standard modes of UVES, DIC1(346+580) and DIC2 (437–860), were used, covering the whole wavelength range ~3050–10400 Å with a gap between ~5770 and 5830 Å due to an inaccurate setting of the optical elements of the spectrograph. Slit widths of 0.″4 and 0.″3 for the blue and red branches, respectively, were applied to satisfy the two pixel criteria for the slit image projection to the corresponding CCD cameras, providing the highest possible resolving power of ~80,000 for the blue and ~110,000 for the red spectrograph branches.

Four highly reddened stars, CD-32 4348, HD 63804, HD 78344, and HD 80077, were exposed 12, 13, 10, and 12 times, with integrated exposure times of 9180, 5350, 7950, and 2160 s, respectively, to record their spectra. Individual spectra discussed in this Letter result from averaging all exposures for each target. The spectra were processed in a standard way using both IRAF packages and our own DECH[5] codes. As shown in Figure 1, in all four spectra, both the strong Na I doublet at ~3302 Å and the relatively weak K I doublet at 4044.142 and 4047.213 Å lack significant Doppler splittings, and therefore, the wavelength scale of each spectrum has been shifted using the Na I doublet at ~3302 Å so that interstellar absorption lines appear at rest wavelengths.

* Based on observations collected at the European Organisation for Astronomical Research in the southern hemisphere, Chile, under program 092.C-0019(A).

[5] http://gazinur.com/DECH-software.html

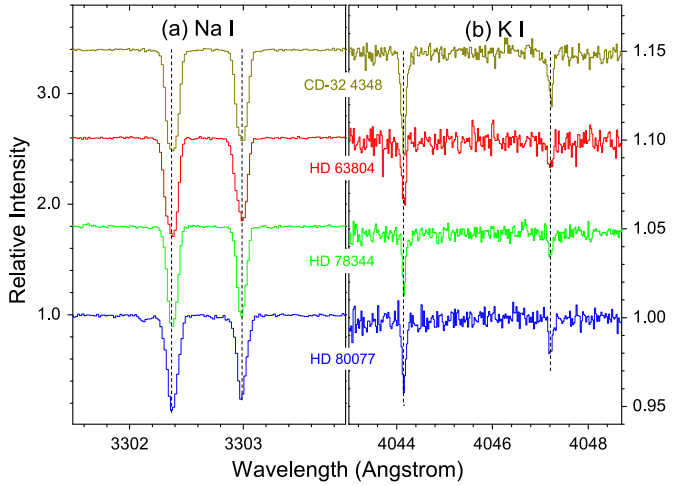

Figure 1. Na I and K I atomic lines. The wavelength scale of each spectrum has been shifted so that interstellar absorption lines appear at rest wavelengths.

3. MOLECULAR DATA

Merer et al. (1975) studied the near-UV spectra of the $A^3\Pi$–$X^3\Sigma^-$ electronic transition system of OH^+ at high resolution in the laboratory and determined accurate molecular constants. In Table 1, we summarize the line positions of electronic transitions from the lowest ground state $N=0$ level in the (0, 0) and (1, 0) bands as measured by Merer et al. (1975). The absolute wavelength accuracy is estimated to be better than 0.01 Å.

Recently, Porras et al. (2014) demonstrated that the $A^3\Pi$–$X^3\Sigma^-$ transition oscillator strengths calculated by de Almeida & Singh (1981) are overestimated, and recommended a value of $f=0.00114$ for the $^rR_{11}(0)$ 3583.76 Å line, which is nearly a factor of three smaller than that in de Almeida & Singh (1981). Therefore, in this work, oscillator strengths of the OH^+ absorption lines listed in Table 1 have been (re)calculated using Pgopher software.[6] In our calculation, the first step is to derive an effective $^3\Pi$–$^3\Sigma^-$ Hamiltonian that reproduces the experimental (0, 0) and (1, 0) band spectra as measured by Merer et al. (1975). Because different definitions for the $A^3\Pi$ v=0 and 1 states are used in Pgopher and in Merer et al. (1975), we refitted the experimental data to determine the input parameters for $A^3\Pi$ v=0 and 1 states in Pgopher. The perturbation in the (1, 0) band (Merer et al. 1975; Rodgers et al. 2007) is also included in the Hamiltonian model. Since the calculations of Hönl–London factors are built-in in Pgopher, the determination of absolute line strengths only requires the transition dipole moment as input. We adopted the $A^3\Pi$–$X^3\Sigma^-$ electronic transition dipole moment (0.3711 Debye) calculated by Merchán et al. (1991), and the Frank–Condon factor $q_{00}=0.626$ calculated by de Almeida & Singh (1981), as these values reproduce well the experimentally determined radiative lifetime of the $A^3\Pi$ v=0 state (Möhlmann et al. 1978). For the (1, 0) band, it is found that the Frank–Condon factor $q_{10}=0.261$, calculated by de Almeida & Singh (1981), cannot reproduce the relative intensities of the two bands in our observational spectra (see Section 4), nor the *ab initio* calculated radiative lifetime of the $A^3\Pi$ $v=1$ state (Merchán et al. 1991). Therefore, we estimate q_{10} from the two $^rR_{11}(0)$ transitions (3583.76 and 3346.96 Å) in our observational spectra, which yields $q_{10}/q_{00}\approx 0.71$, i.e., $q_{10}=0.445$. With these parameters, the effective transition dipole moment for the (0, 0) and (1, 0) bands is inferred as 0.294 and 0.248 Debye, respectively. The resulting line oscillator strengths from our calculation are summarized in Table 1. As can be seen there, our value for the $^rR_{11}(0)$ 3583.76 Å line ($f=0.00102$) is in good agreement with that recommended by Porras et al. (2014).

[6] Pgopher, a Program for Simulating Rotational Structure, C. M. Western, University of Bristol, http://pgopher.chm.bris.ac.uk

Table 1
Line Positions and Oscillator Strengths of OH^+ in the Near-UV

	(0, 0)		(1, 0)	
Transition	λ (Å)	f (10^{-4})	λ (Å)	f (10^{-4})
$^rR_{11}(0)$	3583.757	10.20	3346.961	7.11
$^rQ_{21}(0)$	3572.649	6.03	3337.358	4.16
$^sR_{21}(0)$	3566.445	2.29	3332.177	1.66
$^rP_{31}(0)$	3565.341	2.46	3330.409	1.72
$^sQ_{31}(0)$	3559.807	1.67	3326.368	1.29
$^tR_{31}(0)$	3553.329	0.09	3319.971	0.06

Note. Positions of the two $^tR_{31}(0)$ lines are calculated using molecular constants from Merer et al. (1975).

4. RESULTS AND DISCUSSION

To search for the expected absorption features, the spectra of both bands of OH^+ are calculated for different rotational temperatures $T_{\rm rot}$ ranging from 1 to 8 K in Pgopher. For this $T_{\rm rot}$ range, no substantial differences in spectral appearance are found. This is in agreement with the fact that almost all molecules populate in the $N=0$ level at low $T_{\rm rot}$ (<8 K), e.g., more than 99% are populated in the $N=0$ levels at 8 K. At these low temperatures, all detectable transitions start from the same $N=0$ ground state level and their relative line strengths only depend on oscillator strengths. Because the rotational excitation temperatures of polar molecules in translucent clouds usually do not exceed 5 K, the OH^+ absorption features in the observational spectra can be searched for directly using the calculated spectrum.

Figure 2 shows the spectra of four highly reddened stars (Table 2) in two wavelength regions corresponding to the OH^+ $A^3\Pi$–$X^3\Sigma^-$ (0, 0) and (1, 0) bands, respectively. It should be noted that a few very weak features that, at present, cannot be assigned also show up. Here, we focused on features reasonably overlapping with the accurately predicted OH^+ spectra. It can be found from Figure 2 that, in addition to the previously identified 3583.76 Å feature (Krełowski et al. 2010), the 3572.65 Å line of OH^+ can be identified in all four spectra. Another five transition lines of OH^+ at 3566.45, 3565.34, 3559.81, 3346.96, and 3337.36 Å can also be recognized in the spectra of CD-32 4348 and HD 63804. To unambiguously identify the relatively weak absorption features, the four spectra are averaged to obtain a higher signal-to-noise ratio (S/N). This superposition spectrum represents an average of nearly 50 exposures. As shown in Figure 2, the overall S/N is clearly improved compared to individual spectra. The absorption lines of OH^+ hinted for in the individual spectra now can be clearly seen in the averaged spectrum, with the intensity pattern of each band nearly identical to the calculated spectrum, confirming the origin of these interstellar UV features to be OH^+. The equivalent widths for the two $^rR_{11}(0)$ transitions

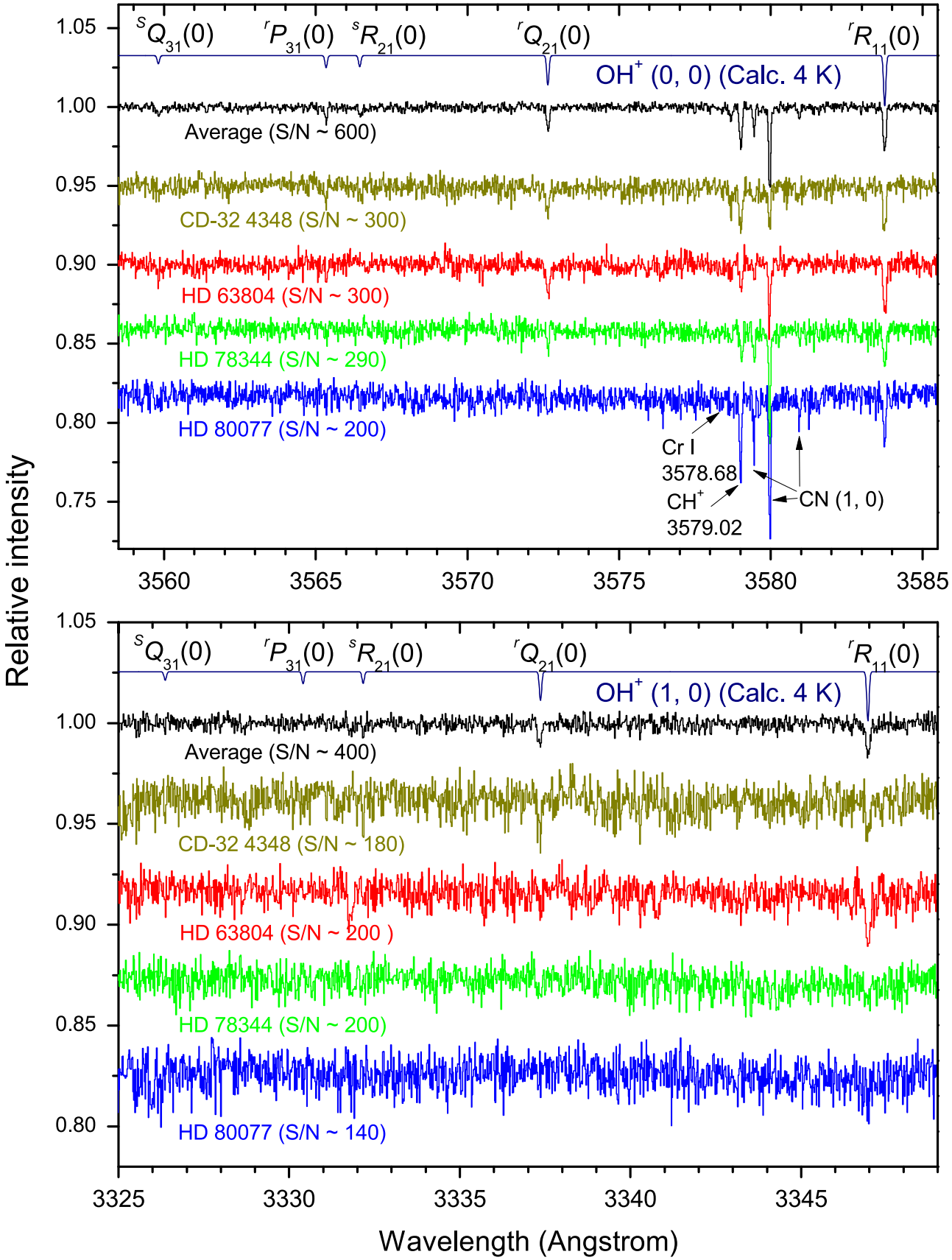

Figure 2. Spectra of the OH^{+} $A^{3}\Pi$–$X^{3}\Sigma^{-}$ (0, 0) and (1, 0) bands. From top to bottom in each panel: calculated 4 K spectrum, averaged spectrum, and individual spectra toward four high reddened stars. Spectra of the observed targets are normalized to pseudo-continuum, i.e., all broad features including stellar lines are eliminated for clarity. The narrow interstellar lines of CH^{+}, Cr I, and CN are marked in the upper panel. The overall S/N estimated from the displayed wavelength regions are also presented for each spectrum.

Table 2
Targets and Measured Molecular Data

	CD-32 4348	HD 63804	HD 78344	HD 80077
Target Properties[a]				
Sp/L	B7Iab	A0Ia(p)	O9.5Ia	B2Ia
V	8.91	7.75	8.94	7.56
$E(B-V)$	1.14	1.19	1.33	1.50
Equivalent Widths (mÅ)[b]				
3583.76	3.53 ± 0.29	4.32 ± 0.30	2.86 ± 0.40	3.05 ± 0.37
3572.65	2.40 ± 0.31	2.78 ± 0.21	1.34 ± 0.23	1.35 ± 0.22
3566.45	1.00 ± 0.33	(0.95)	(0.98)	1.01(1.20)
3565.34	1.23 ± 0.35	1.34 ± 0.36	0.88(0.98)	(1.20)
3559.81	(0.95)	(0.95)	(0.98)	(1.20)
3346.96	2.41 ± 0.38	3.32 ± 0.45	1.16(1.34)	1.64(1.70)
3337.36	1.87 ± 0.50	1.41 ± 0.30	1.15(1.34)	(1.70)
$N(OH^+)$	3.40 ± 0.17	4.04 ± 0.22	2.38 ± 0.13	2.51 ± 0.17
N(K I)	0.75 ± 0.06	0.57 ± 0.12	0.36 ± 0.06	0.55 ± 0.07
ζ_p	0.8	1.2	0.8	0.9

Notes. Values of $N(OH^+)$ and N(K I) are in units of 10^{13} cm^{-2}, and ζ_p in 10^{-16} s^{-1}. The ζ_p-values are inferred using Equation (2).
[a] Spectral types and V magnitudes of target stars are taken from Walker (1963), Buscombe (1969), MacConnell & Bidelman (1976), Houk (1982), and Schild et al. (1983), and $E(B-V)$ magnitudes are determined using intrinsic colors from Papaj et al. (1993).
[b] The uncertainties of equivalent widths are one standard deviation (1σ) following a Gaussian profile fitting. Italic numbers indicate tentatively detected lines. For tentatively detected and non-detected lines, the numbers in parenthesis give the 3σ upper limits that are estimated from the continuum S/N.

(3583.76 and 3346.96 Å) in the averaged spectrum are used to estimate the Frank–Condon factor ratio q_{10}/q_{00} discussed before. The line equivalent widths in individual spectra are summarized in Table 2. Weak features that are only tentatively detected in spectra of HD 78344 and HD 80077, i.e., lines with equivalent widths slightly below the 3σ upper limits, are also listed in Table 2.

It should be noted that, very recently, the 3572.65 Å and 3346.96 Å features, identified as OH^+ absorption lines here, were also detected (but not identified) by Bhatt & Cami (2015) in an averaged spectrum of a large number of archived VLT/UVES data. They also reported tentative detections of the 3346.96 Å feature in individual targets of HD 115363, HD 142758, HD 188220, HD 210121, and HD 143448.

Since all observed transitions (Table 2) start from the same $N=0$ ground state level, we determine OH^+ column densities $N(OH^+)$ by a linear fit of equivalent widths (W_λ) to ($\lambda^2 f$), using the equation

$$W_\lambda = 8.853 \times 10^{-18} * N\left(OH^+\right) * \left(\lambda^2 f\right) \quad (1)$$

where $N(OH^+)$ is in cm^{-2}, W_λ in mÅ, and λ in Å. Figure 3 shows the fitting result for all four targets. The linearity of the fits for CD-32 4348 and HD 63804 further confirms the reliability of the newly determined Frank–Condon factor q_{10}. Moreover, such a linear fit comprising a larger set of observational data in each target allows one to determine the OH^+ column density more precisely than using the 3583.76 Å line only. The resulting column densities are listed in Table 2.

The derived OH^+ column densities in Table 2, subsequently, offer a diagnostic tool to infer the primary cosmic ray ionization rate ζ_p in the studied translucent clouds, using the approximate equation given by Porras et al. (2014),

$$\zeta_p \approx 1.33 \times 10^{-8} * N\left(OH^+\right)/N\,(H), \quad (2)$$

for typical physical settings corresponding to a UV field[7] $\chi = 1$ and $n_H = 100$ cm^{-3}. As in Porras et al. (2014), N(H) ($=N$(H I) + 2*$N(H_2)$) in Equation (2) is estimated from N(K I) in each target using the relationship described by Welty & Hobbs (2001). Here we determine N(K I) using the K I doublet at 4044.142 and 4047.213 Å as shown in Figure 1 and the resulting N(K I) values are given in Table 2. It is important to realize that this procedure may lead to a factor of two uncertainty in the estimated N(H) values (see Figure 17 in Welty & Hobbs 2001). With this procedure, very similar values of $\zeta_p \approx 1.0 \pm 0.2 \times 10^{-16}$ s^{-1} are inferred (see Table 2).

These derived ζ_p-values are consistent with the more complete model concerning effects of polycyclic aromatic hydrocarbon species on ionization by Hollenbach et al. (2012). Their model shows that $N(OH^+)$ approaches a saturation when the total optical extinction $A_{v,t}$ is close to and larger than 1.0 in a diffuse/translucent cloud, in which case the value of $N(OH^+)$ mainly depends on ζ_p/n_2 (the unitless parameter $n_2 = n_H/100$ cm^{-3}). Taking the equivalent color excess ($E(B-V)$) values of our targets (Table 2) and the typical total to selective extinction ratio $R=3.1$, we find that in all cases $A_{v,t}$ is larger than 3.0 mag. In this case, we can approximately estimate the primary cosmic ray ionization rate ζ_p, based on Figures 10 and 11 in Hollenbach et al. (2012). Using our derived values of $N(OH^+)$, we obtain a typical value of $\zeta_p \approx 1.1 \pm 0.3 \times 10^{-16}$ s^{-1}, which is in good agreement with the values listed in Table 2.

Our estimation of the ζ_p-value is based on the assumption of a single cloud in the line of sight. However, the absorption line width of OH^+ in all four spectra, typically ~10 km s^{-1}, is significantly larger than the instrument resolution of UVES, suggesting that geometrical effects such as observing several clouds along the line of sight, or viewing the cloud obliquely, cannot be excluded. Because of this and the possible variation of the assumed parameters χ and n_H, the error of the estimated ζ_p-value may actually be much larger. However, we find that our results are within the range of ζ_p-values inferred in other diffuse/translucent clouds, e.g., ~0.6–3.5 × 10^{-16} s^{-1} from HIFI observations of OH^+ and H_2O^+ (Neufeld et al. 2010; Indriolo et al. 2012, 2015), and ~0.3–4.4 × 10^{-16} s^{-1} from detections of H_3^+ in various diffuse/translucent clouds (Le Petit et al. 2004; Indriolo et al. 2007; Indriolo & McCall 2012).

5. CONCLUSIONS

We have presented the detection of the OH^+ $A^3\Pi$–$X^3\Sigma^-$ (0, 0) and (1, 0) bands in four translucent interstellar clouds toward CD-32 4348, HD 63804, HD 78344, and HD 80077. In total, seven absorption features of OH^+ are unambiguously detected in the averaged spectrum of the four sources and six of them are identified for the first time. An accurate determination of OH^+ column densities allows one to infer the primary cosmic ray ionization rate to be of a typical value of ~1.0 × 10^{-16} s^{-1} in the four OH^+-rich translucent clouds studied here. Our results allow

[7] The same as in Hollenbach et al. (2012), $\chi = 1$ corresponds to $G_0 = 1.7$ in the Tielens & Hollenbach (1985) units based on the Habing (1968) local interstellar radiation field.

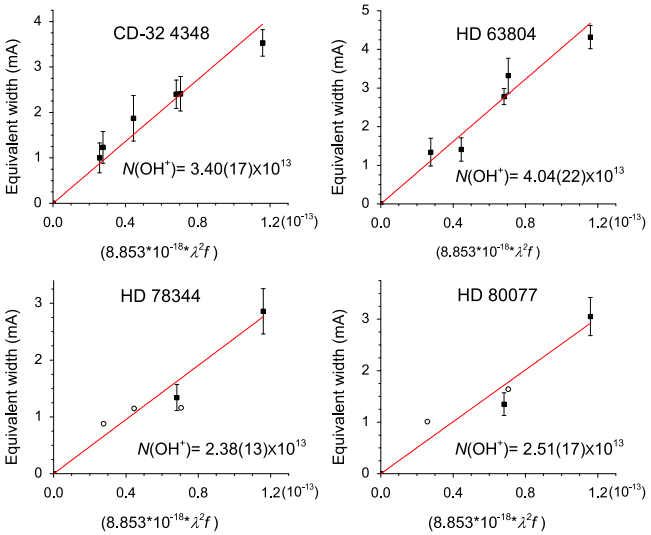

Figure 3. Weighted linear fits of measured equivalent widths to determine OH^+ column densities in the four translucent clouds studied here. Empty circles represent the tentatively detected lines that are not included in the fits.

us to identify two interstellar absorption features, recently reported by Bhatt & Cami (2015) toward sources different from those studied here, as originating from OH^+. Given the role OH^+ is supposed to play in the gas phase formation schemes of water, the present findings may help to link water abundances in the diffuse ISM to the gas phase ion chemistry, specifically, because solid-state water formation schemes (Ioppolo et al. 2008) are not expected to be relevant.

D.Z. and H.L. acknowledge the support from NWO (VICI grant, and Dutch Astrochemistry Network) and NOVA. J.K. acknowledges the financial support of the Polish National Center for Science (grant UMO-2011/01/BST2/05399). G.A.G. acknowledges the support of Chilean fund FONDECYT-regular (project 1120190). We are grateful for the assistance of the Paranal Observatory staff members. We thank Dr. Western (Bristol) for the useful discussion in the calculations of oscillator strengths using Pgopher.

REFERENCES

Barlow, M. J., Swinyard, B. M., Owen, P. J., et al. 2013, Sci, 342, 1343
Bhatt, N. H., & Cami, J. 2015, ApJS, 216, 22
Buscombe, W. 1969, MNRAS, 144, 31
de Almeida, A. A., & Singh, P. D. 1981, A&A, 95, 383
Gerin, M., De Luca, M., Black, J., et al. 2010, A&A, 518, L110
Gredel, R., Carpentier, Y., Rouillé, G., et al. 2011, A&A, 530, A26
Habing, H. J. 1968, BAN, 19, 421
Hollenbach, D., Kaufman, M. J., Neufeld, D., Wolfire, M., & Goicoechea, J. R. 2012, ApJ, 754, 105
Houk, N. 1982, Michigan Catalogue of Two-dimensional Spectral Types for the HD Stars, Vol. 3 (Ann Arbor, MI: Univ. Michigan Press)
Indriolo, N., Geballe, T. R., Oka, T., & McCall, B. J. 2007, ApJ, 671, 1736
Indriolo, N., & McCall, B. J. 2012, ApJ, 745, 91
Indriolo, N., Neufeld, D. A., Gerin, M., et al. 2012, ApJ, 758, 83
Indriolo, N., Neufeld, D. A., Gerin, M., et al. 2015, ApJ, 800, 40
Ioppolo., S., Cuppen, H. M., Romanzin, C., van Dishoeck, E. F., & Linnartz, H. 2008, ApJ, 686, 1474
Krełowski, J., Beletsky, Y., & Galazutdinov, G. A. 2010, ApJL, 719, L20
Le Petit, F., Roueff, E., & Herbst, E. 2004, A&A, 417, 993
MacConnell, D. J., & Bidelman, W. P. 1976, AJ, 81, 225
Merchán, M., Malmqvist, P.-Å., & Roos, B. O. 1991, AcTC, 79, 81
Merer, A. J., Malm, D. N., Martin, R. W., Horani, M., & Rostas, J. 1975, CaJPh, 53, 251
Möhlmann, G. R., Bhutani, K. K., de Heer, F. J., & Tsurubuchi, S. 1978, CP, 31, 273
Neufeld, D. A., Goicoechea, J. R., Sonnentrucker, P., et al. 2010, A&A, 521, L10
Papaj, J., Krełowski, J., & Wegner, W. 1993, A&A, 273, 575
Porras, A. J., Federman, S. R., Welty, D. E., & Ritchey, A. M. 2014, ApJ, 781, 8
Rodgers, D. J., Batey, A. D., & Sarre, P. J. 2007, MolPh, 105, 849
Schild, R. E., Garrison, R. F., & Hiltner, W. A. 1983, ApJS, 51, 321
Tielens, A. G. G. M. 2013, RvMP, 85, 1021
Tielens, A. G. G. M., & Hollenbach, D. 1985, ApJ, 291, 722
van der Tak, F. F. S., Nagy, Z., Ossenkopf, V., et al. 2013, A&A, 560, A95
van Dishoeck, E. F., Herbst, E., & Neufeld, D. A. 2013, ChRv, 113, 9043
Walker, G. A. H. 1963, MNRAS, 125, 141
Welty, D. E., & Hobbs, L. M. 2001, ApJS, 133, 345
Wyrowski, F., Menten., K. M., Guesten., R., & Belloche, A. 2010, A&A, 518, 26